ASTROBIOLOGY
Volume 14, Number 5, 2014

DOI: 10.1089/ast.2013.1081

# Field Trial of a Dual-Wavelength Fluorescent Emission (L.I.F.E.) Instrument and the Magma White Rover during the MARS2013 Mars Analog Mission

Gernot Groemer,[1,2] Birgit Sattler,[1] Klemens Weisleitner,[1] Lars Hunger,[3] Christoph Kohstall,[4] Albert Frisch,[5] Mateusz Józefowicz,[6] Sebastian Meszyński,[6,7] Michael Storrie-Lombardi,[8,9] and the MARS2013 Team

**Abstract**

We have developed a portable dual-wavelength laser fluorescence spectrometer as part of a multi-instrument optical probe to characterize mineral, organic, and microbial species in extreme environments. Operating at 405 and 532 nm, the instrument was originally designed for use by human explorers to produce a laser-induced fluorescence emission (L.I.F.E.) spectral database of the mineral and organic molecules found in the microbial communities of Earth's cryosphere. Recently, our team had the opportunity to explore the strengths and limitations of the instrument when it was deployed on a remote-controlled Mars analog rover. In February 2013, the instrument was deployed on board the Magma White rover platform during the MARS2013 Mars analog field mission in the Kess Kess formation near Erfoud, Morocco. During these tests, we followed tele-science work flows pertinent to Mars surface missions in a simulated spaceflight environment. We report on the L.I.F.E. instrument setup, data processing, and performance during field trials. A pilot postmission laboratory analysis determined that rock samples acquired during the field mission exhibited a fluorescence signal from the Sun-exposed side characteristic of chlorophyll *a* following excitation at 405 nm. A weak fluorescence response to excitation at 532 nm may have originated from another microbial photosynthetic pigment, phycoerythrin, but final assignment awaits development of a comprehensive database of mineral and organic fluorescence spectra. No chlorophyll fluorescence signal was detected from the shaded underside of the samples. Key Words: Biosensor—Life-detection instruments—Mars—Biomarkers—Planetary protection. Astrobiology 14, 391–405.

## 1. Introduction

Mars may have once had the prerequisites for the emergence of life, including liquid water, a warmer and denser atmosphere, an intact planetary magnetic field, and a chemistry similar to that of early Earth (*e.g.,* Jakosky and Phillips, 2001; Bishop *et al.,* 2013). But Viking data indicate that today the surface of Mars lacks even infall organics, most likely due to destruction by ultraviolet and heavy particle radiation (Biemann *et al.,* 1976). Recent simulations predict that microbial life would have had to reside several meters below the surface if it were to have survived heavy particle bombardment for geologically significant time periods (Dartnell *et al.,* 2007).

However, increased understanding of the viability envelopes of microbial organisms in extreme environments on Earth has contributed to the development of models for putative Mars ecosystems (*e.g.,* Jepsen *et al.,* 2007; Warner and Farmer, 2010). In such models, subsurface habitable niches are proposed such as the martian permafrost (McKay *et al.,* 2013), portions of the regolith hidden beneath translucent glaciers in the polar regions (Fisher and Schulze-Makuch, 2013), volcano-ice boundary zones (Cousins and Crawford, 2011), the subsurface ice beneath polygonal

[1]Institute of Ecology, University of Innsbruck, Innsbruck, Austria.
[2]Austrian Space Forum, Innsbruck Office, Innsbruck, Austria.
[3]Institute of Astro- and Particle Physics, University of Innsbruck, Innsbruck, Austria.
[4]Physics Department, Stanford University, Stanford, California, USA.
[5]Institute of Experimental Physics, University of Innsbruck, Innsbruck, Austria.
[6]ABM Space Education, Toruń, Poland.
[7]Department of Informatics, Nicolaus Copernicus University, Toruń, Poland.
[8]Kinohi Institute, Pasadena, California, USA.
[9]Department of Physics, Harvey Mudd College, Claremont, California, USA.

terrain (Wilhelm *et al.,* 2012), and the interior of lava tubes (Leveille and Datta, 2010; Northup *et al.,* 2011 and Popa *et al.,* 2012). Such models have fueled interest in developing instrument suites capable of rapidly characterizing the mineral and organic composition of these niche environments during robotic or astronaut exploration.

Interestingly, the search for instruments capable of detecting organics on Mars has cross-fertilized the field of extremophile research on Earth, encouraging and enabling the search for habitats in the cryosphere (Psenner and Sattler, 1998; Psenner *et al.,* 2003; Priscu, 2009), high-altitude cloud water droplets (Sattler *et al.,* 2001), and permafrost brine pockets (Gilichinsky *et al.,* 2003). The majority of these habitats are ultra-oligotrophic, which places them at extreme risk for overgrowth by contaminating organisms introduced during exploration, particularly when working with invasive, contact-rich sample manipulation methods. Noncontact, nondestructive, non-invasive detection methods are preferred for these fragile ecosystems, and first-generation imaging and spectroscopy systems have been developed and tested in extreme environments such as the Atacama Desert (Vítek *et al.,* 2010) and Antarctica (Storrie-Lombardi and Sattler, 2009a, 2009b; Sattler *et al.,* 2010).

The overarching goal of our team is the development of a suite of optical survey instruments that avoid human or robotic direct contact with either geological or biological targets of interest and do not require the use of irreplaceable consumables. The instruments under investigation by the members of our group include optical wavelength imaging, fluorescence imaging and spectroscopy, and Raman spectroscopy. Visible light or fluorescence images can be acquired quickly, provide context, and make possible the preliminary detection of a region of interest, but they usually provide relatively minimal chemical specificity. On the other end of the scale, the Raman spectrometers commonly employed for extreme environment characterization generate single point spectral data and require a longer data acquisition time but can provide relatively unambiguous chemical identification for mineral and organic species. Fluorescence spectra elicited at multiple wavelengths occupy a middle ground. They can be obtained relatively rapidly and, if evaluated in the context of an extensive mineral and organic fluorescence spectral data set, can provide preliminary chemical information about a region of interest sufficient to identify at least families of organic molecules and mineral species. For example, with two wavelengths as probes and a reliable comparison data set, sufficient spectral information can be obtained to identify specific bacterial species including biowarfare agents (Farsund *et al.,* 2012). Fluorescence response evaluated across time can be used to detect radiation damage to a putative organic target (Dartnell *et al.,* 2011, 2012). Time-resolved fluorescence can effectively discriminate between organic and inorganic targets on the basis of fluorescence lifetime, or detect the presence of metabolic activity (Alimova *et al.,* 2003).

In final mission format, the instrument suite should include all these modalities: visible imaging, fluorescence imaging, fluorescence spectra, and Raman spectra employing lasers at multiple wavelengths. For example, while Raman spectroscopy is sensitive to the bulk structure of minerals, it is insensitive to trace metal ions in the crystal lattice. Using a combined fluorescence and Raman system operating at 266, 355, and 532 nm, Bozlee *et al.* (2005) demonstrated that remote laser-induced fluorescence of rocks and minerals can be a useful technique for detecting the presence of trace cations in minerals and provides complementary information to Raman probes.

In a similar fashion, noting that laser-induced fluorescence and time-resolved fluorescence can measure trace amounts of transition metal ions and rare-earth ions from light rare-earth elements such as cerium (Ce) to heavy rare-earth elements such as ytterbium (Yb) and that fluorescence is one of the most sensitive techniques for detecting polyaromatic hydrocarbons (PAHs), Abedin *et al.* (2013) proposed a prototype fluorescence and Raman system capable of determining the distribution of trace fluorescent ions, revealing the geological conditions under which minerals formed on the surface and subsurface of Mars, and screening for low levels of subsurface organics. Laser wavelengths proposed for this system are 355, 532, and 1064 nm.

The instruments employed for the MARS2013 mission included visible wavelength imaging for target context with an onboard rover RGB camera and laser-induced fluorescence emission (L.I.F.E.) spectra elicited by excitation with 405 and 532 nm laser diodes. For work in extreme environments on Earth, these two wavelengths are of particular utility because they target the absorption bands of chlorophylls, carotenoids, and the phycobiliproteins in photosynthetic microorganisms. With the exception of the Mars glacier niche described above, these applications of the two wavelengths are not why they are useful during Mars exploration. Laser excitation at 532 nm is of utility to identify fluorescence in targets that may complicate acquisition and interpretation of Raman spectral data generated at that wavelength by Raman remote interrogation systems currently under development (Sharma *et al.,* 2009). Laser excitation at 405 nm is of particular utility as a Mars survey tool because it targets a radiation-resistant molecular structure found in all microbial species investigated to date: the porphyrin ring, which is fundamental to the construction of the metabolic biomolecules known as cytochromes. The ubiquity and stability of the porphyrin ring following the death of the parent organism has resulted in its nomination as the ''ideal biomarker'' for both fossil and extant life (Suo *et al.,* 2007).

Merging such noncontact, nondestructive spectral data acquisition technology with robotic systems may be of particular benefit for surveys of Earth's deserts and cryosphere. Until recently, extreme environment field work has required extensive human ''hands-on'' operation both for initial data collection and signal extraction. A robotic, automated system working in real time would make these optical techniques useful for rapidly screening large areas of sensitive habitats such as hot and cold deserts and areas that are inaccessible for human exploration. The merger of optical and robotic technologies could produce surveys that impart minimal disturbance to a fragile ecosystem and allow investigators to bring home only those samples shown to be rich in target biomolecules. Such studies have slowly begun to appear and are adding significant information about some of the most remote environments on Earth (Warren-Rhodes *et al.,* 2007).

In this paper, we report on a field trial of this strategy for low-cost, high-resolution, noncontact data collection during

Mars analog robotic field trials in the northern Sahara Desert. We first describe the field site, discuss the choice of lasers, present the design of our L.I.F.E. spectrometer, and describe the Magma White rover that carries the spectrometer. We discuss the impact of the scientific instrument on the work flows specific to modeled spaceflight, time-delayed operational constraints during a Mars analog mission.

## 2. The MARS2013 Field Simulation

February 1 through 28, 2013, the Austrian Space Forum (Österreichisches Weltraum Forum, OeWF) conducted the MARS2013 field simulation, an integrated high-fidelity Mars analog mission in the Moroccan Sahara near Erfoud (31°21′N, 04°04′E, see Fig. 1) in the Laghdad Ridge, Tafilalt region in the eastern Anti-Atlas. Supported by a Mission Support Center (MSC) in Innsbruck, Austria, 17 experiments relevant for Mars exploration projects were conducted exercising realistic tele-operation and tele-science work flows in a simulated operational spaceflight environment (Groemer *et al.,* 2014 in this issue).

This site was chosen for its environmental conditions being compatible with the operational envelope of the MARS2013 experiment hardware, terrain diversity allowing for a wide range of robotic tests concerning trafficability as well as long-range telemetry tests, and available technical infrastructure.

The geological setting is dominated by a Precambrian crystalline basement and a thick deformed upper-Precambrian and Paleozoic layer, and overlain by an undeformed Cretaceous and Tertiary sedimentary rocks. During the Paleozoic, mud mounds were hydrothermally (Mounji *et al.,* 1998) formed in this region, which represent the topmost part of the Kess Kess Formation, an Early Devonian crinoidal limestone with underlying volcanic sediments (Belka, 1998). As such, they represent a model system for mud volcanoes on Mars (Skinner and Mazzini, 2009). For an overview on the Laghdad Ridge geology, we refer to the work of Cavalazzi (2006).

### 2.1. Fluorescence technique

Fluorescence spectroscopy is based on optical emission of photons from molecules that have been excited to higher energy levels by the absorption of electromagnetic radiation. The fluorescence is the spontaneous emission of lower-energy photons from these photon-activated molecules. This technique has the potential for greater specificity than absorption methods, is easier to implement remotely, and can

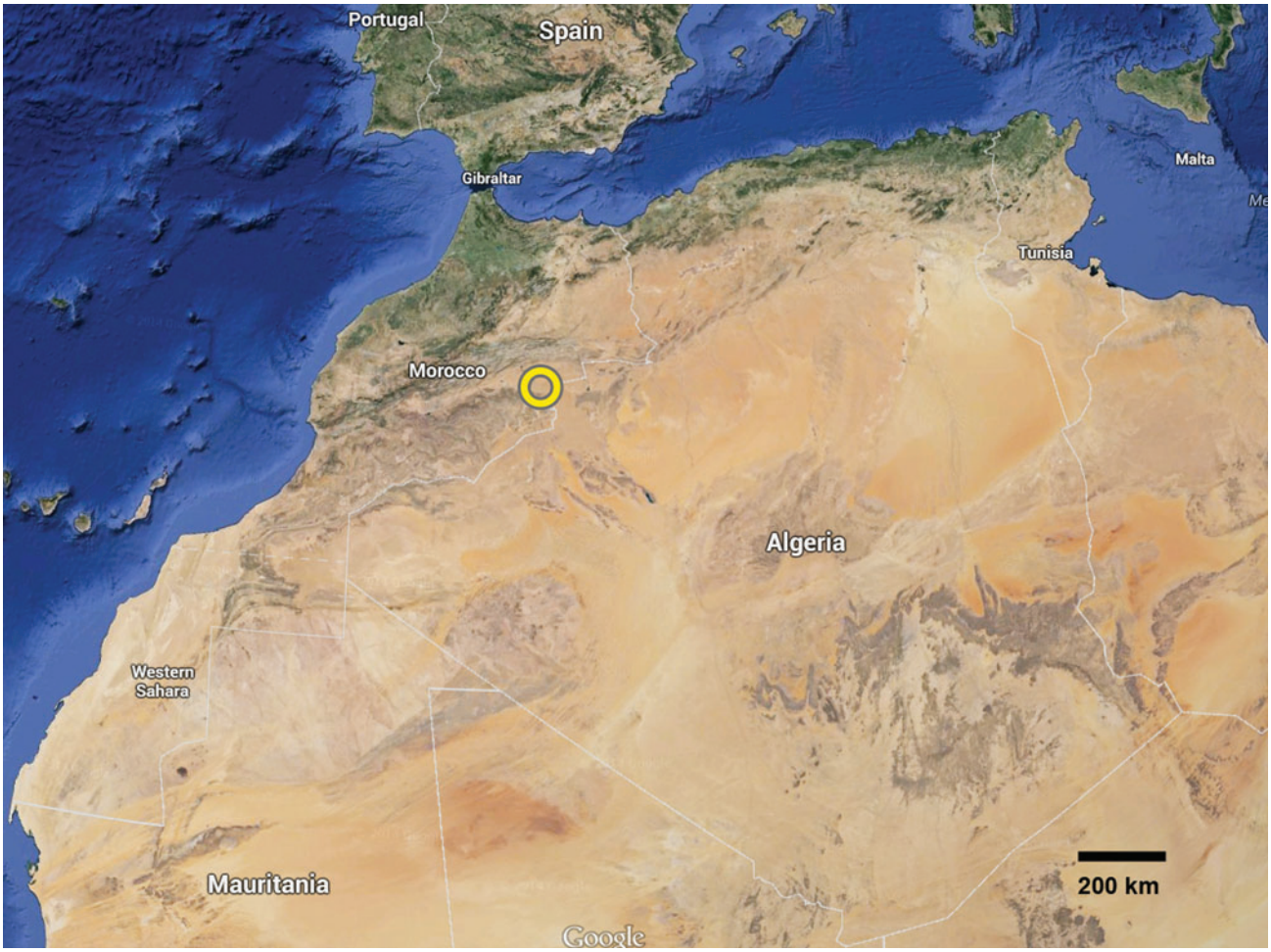


**FIG. 1.** The MARS2013 test site was located at 31°21′N, 04°04′E, near the city of Erfoud, Morocco. Color images available online at www.liebertonline.com/ast

be used to investigate the electronic structure of mineral defects, detect fluorescent ions in mineral species, and make quantitative estimates of the concentrations of fluorescent activity centers in minerals. Laser-induced fluorescence and time-resolved fluorescence can measure trace amounts of transition metal ions and rare-earth ions. Fluorescence is one of the most sensitive techniques for detecting PAHs and biomolecular species containing aromatic structures, which have high fluorescence quantum yields if the excitation wavelength falls within the primary absorption bands of the target. Fluorescence cross sections can be up to 9 orders of magnitude greater than Raman scattering cross sections.

Laser-induced fluorescence emission techniques have previously been employed to detect bacteria in Mars analog soils (Storrie-Lombardi *et al.,* 2001), find previously unknown microorganisms in deep subsurface Hawaiian basalts (Fisk *et al.,* 2003), define PAH detection limits for the ExoMars rover (Storrie-Lombardi *et al.,* 2008, 2009), and discover microbial life inhabiting the ice covers of Antarctic lakes (Sattler and Storrie-Lombardi, 2009; Storrie-Lombardi and Sattler, 2009a, 2009b; Sattler *et al.,* 2010). Illumination of microbial life when using a 405 nm laser excitation produces a fluorescence response from a variety of intracellular biomolecules based on a single structure, the porphyrin ring. Cellular metabolism and the evolution of cellular chemistry are intimately entwined with the interaction between organic molecules and metal ions. The porphyrin molecular structure is comprised of four linked pyrrole rings, whose four interior nitrogens are available to coordinate a metal cation. Porphyrin molecules are central to cellular metabolism for species across all branches of the tree of life. They take part in multiple chemical pathways including energy transfer (cytochrome with an iron central cation), energy conversion (chlorophyll with magnesium), and oxygen transfer (hemoglobin with iron), and in a variety of enzymes such as cobalamin (vitamin B12) containing a cobalt cation.

Due to its ubiquity, resistance to physical degradation, and survival when exposed to high levels of ionizing radiation, the porphyrin ring has been proposed as the ideal biomarker for detection of extant or ancient life on Earth or other terrestrial bodies (Suo *et al.,* 2007). Molecular species containing the ring typically exhibit absorption maxima near 410 nm and produce a broad fluorescence response between 430 and 550 nm in organisms exposed to 405 nm laser illumination (Stramski and Kiefer, 1998; Bhatta *et al.,* 2005). Although of relatively minimal importance for the exploration of the martian regolith, on Earth the most commonly encountered photosynthetic porphyrin derivatives are the chlorophylls. Microbial and plant chlorophylls characteristically exhibit a prominent absorption band between 400 and 450 nm. Cyanobacteria that inhabit alkaline lake tufas exhibit strong L.I.F.E. signatures between 450 and 750 nm with maxima at 540 and 660 nm following excitation by a 405 nm laser (Storrie-Lombardi *et al.,* 2011).

Laser excitation at 532 nm targets photosynthetic pigments known as the phycobiliproteins, accessory pigments found primarily in red algae, cyanobacteria, and cryptomonads (Samsonoff and MacColl, 2001). The phycobiliproteins exhibit strong absorption bands between 480 and 560 nm. Laser excitation at 532 nm of cyanobacteria-dominated assemblages living within the ice of ancient Antarctic lakes produces autofluorescence activity between 560 and 730 nm. The L.I.F.E. signature is attributed to the presence of the phycobiliprotein known as phycoerythrin (Storrie-Lombardi and Sattler, 2009a, 2009b). L.I.F.E. spectral signatures of ocean and lake phytoplankton have been obtained from airborne platforms such as NASA's Airborne Oceanographic LIDAR (Light Detection and Ranging) for more than three decades by using 532 nm excitation (Hoge and Swift, 1981; Hoge *et al.,* 1998). L.I.F.E. signatures have been obtained from microbes living in Alaskan river ice by using a small 532 nm, 5 mW laser diode housed in a single-engine plane flying at an altitude of approximately 100 m (Storrie-Lombardi and Sattler, 2009a, 2009b).

### 2.2. L.I.F.E. instrument

We have developed a portable fluorescence spectrometer utilizing two lasers (Fig. 2). With one shot, the spectrometer analyzes a full line on the specimen and records the spectral information for every point on this line with a resolution of approximately 5 nm. Excitation is accomplished by using 5 mW of linear polarized light at 532 nm or 5 mW of linear polarized light at 405 nm generated by two commercially available laser pens. The two beams are folded into the optical axis with a dichroic mirror. To excite a highly elliptical region on the sample, the beams are expanded by a cylindrical lens in one direction. The beams are aligned with the optical axis of the spectrometer by using a polarizing beam splitter cube (PBS). An exchangeable lens focuses the excitation light onto the sample and creates an elliptical spot with an aspect ratio of 50:1. The exchangeable lens also collects the fluorescent light from the sample. Half the unpolarized collimated fluorescent light passes the beam splitter and is focused onto a slit aperture by a lens system with a demagnification factor of about 2.7. The slit aperture is constructed by two knife edges, of which one is movable while the other is fixed. By increasing the slit aperture size, the amount of collected fluorescent light can be increased but for the price of a reduction in spectral resolution. The slit aperture is then imaged onto a CCD camera by using a second telescope with a demagnification factor of about 2.7. We use a grayscale industrial camera (mvBlueFOX-220G from MatrixVision) with a high conversion resolution of 12 bits and an output resolution of 10 bits connected via USB to the computer. The pixel size of the camera is $5.6 \times 5.6\ \mu m^2$. The prism is oriented perpendicular to the slit aperture so that the two-dimensional CCD captures an image that shows the spectral information in one direction versus the spatial position of the sample in the other direction (see Fig. 2 inset). Two longpass (LP) filters can be placed in front of the slit aperture with a servo motor to filter the excitation laser. The two filters have a cutoff wavelength of 450 and 550 nm for blue and green excitation, respectively. A webcam is used to monitor the probe in color. Targets can be illuminated by ambient light or by a white LED.

2.2.1. Data reduction. The spectrometer is portable and has to be connected to a computer for controlling purposes and recording the CCD images. A microcontroller circuit controls the lasers and rotates the filter wheel with a servo motor. The control sequence of the data acquisitioning was programmed with LabView; the data reduction work flow was implemented as a Matlab code. The LabView code runs

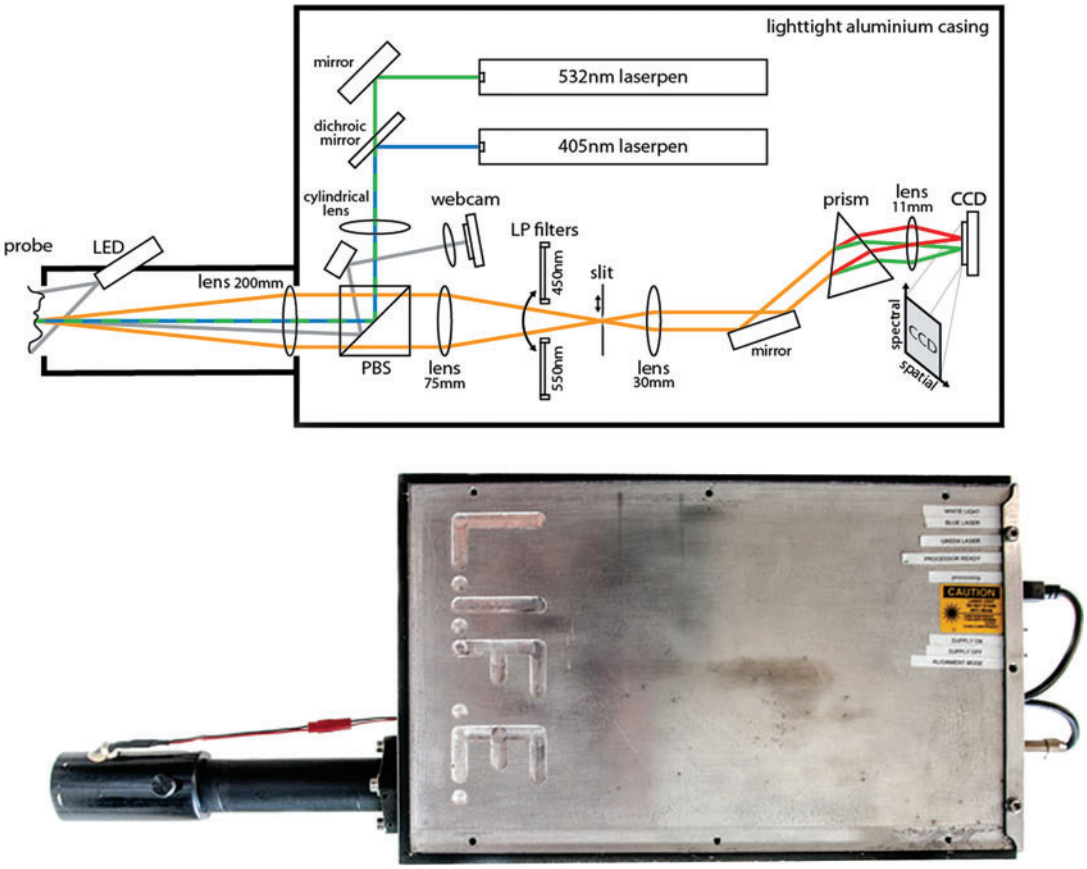


**FIG. 2.** Optical setup of the L.I.F.E. spectrometer and physical realization. Color images available online at www.liebertonline.com/ast

automatically in a predefined data collection sequence. One data set contains 4 pictures with a size of 300 kb each and a log file. The storage/uplink requirement for one dataset is around 1.2 Mb. The data processing work flow consists of two parts, which are (a) creating a dewarp line and wavelength calibration from a calibration picture and (b) dewarping and analyzing pictures.

First, the spectra taken with the L.I.F.E. instrument are two-dimensional spectra, where wavelength is separated along the *x* axis, and the *y* axis gives the spatial coordinate. The resulting spectra are dewarped and wavelength-calibrated, and the background is subtracted. The wavelength calibration is done with the help of the two reference lines of the green laser. The green laser light (532 nm) is produced by frequency doubling of an infrared laser (1064 nm). Calibration pictures are taken without a filter and with short exposure times. On these pictures, we see both wavelengths of the green laser (532, 1064 nm), and with these two lines we then calculate the wavelength information for every pixel on the CCD. Then the picture is cropped again, down to the wavelength range given by the user. The sum of all light within this wavelength range is then plotted along the spatial coordinate to give a rough estimate of how much pigment per area (*e.g.,* $cm^{-2}$) can be seen from the specimen. After this, a spectrum within the given wavelength range is plotted at a spatial position specified by the user. An example of the result of the data reduction is given in Fig. 3.

### *2.3. Laboratory calibration*

As described by Tilg *et al.* (2011) and Sattler *et al.* (2010), calibration for phycoerythrin and chlorophyll has been done with commercial standards (Invitrogen and Sigma-Aldrich). Prior tests have been done with laser pens (< 5 mW) and digital photography where the raw files have been converted via ImageJ into data that is adequate for the fluorescence signal.

Here, we present the laboratory calibration for the phycoerythrin detection and quantification with the 532 nm (green) laser. The L.I.F.E. instrument cannot directly measure concentrations of fluorescent pigments in the samples investigated though it does image the area density of a given pigment. In thin films, this is simply the concentration of pigments per area ($ng/cm^2$). In a column of solution, however, the area density is calculated by multiplying the height of the water column with the concentration of the pigment in the solution. In our calibration, we measured the response signal for solutions of phycoerythrin with a known concentration and column height. We measured 10 different concentrations (5, 10, 20, 40, 80, 160, 320, 640, 800, and 1000 $ng/cm^3$) at three different column heights (1.5, 3.0, and 4.5 cm). Because of geometrical constraints, the measurements taken with lower (1.5 and 3.0 cm) column densities were taken with distances 1.5 and 3.0 cm to the focal point of the instrument; this had to be corrected for during the data

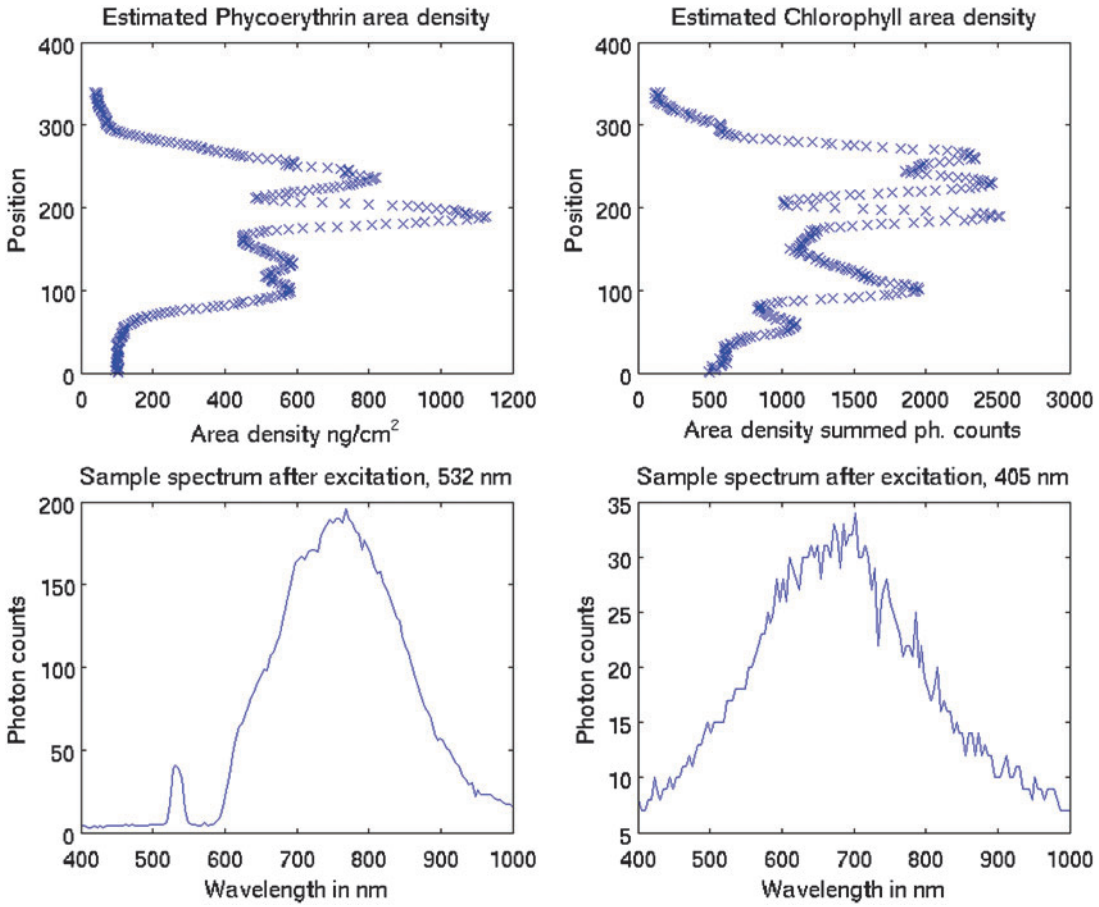


**FIG. 3.** Example of the result of the automated analysis. The data show the sunlit side of the rock as seen in Section 3. In the top left, the estimated area density of phycoerythrin is shown against the position on the measured line (to see spatial variations). The top right shows the same for chlorophyll, showing the photon counts. In the bottom left, the spectrum obtained after 532 nm excitation at the brightest position is given. The bottom right shows the spectrum after 405 nm excitation, also at the brightest position. Color images available online at www.liebertonline.com/ast

reduction. The calibration measurements were taken with different exposure times to get a sufficient signal-to-noise ratio for dim measurements and to prevent detector saturation for bright measurements. For each data point, we summed up the measured counts in the spectral range from 600 to 1000 nm. All the measurements were normalized to a 1 s exposure time during the data reduction. In Fig. 4, we show the phycoerythrin response measured for our three different column heights scaled to the equivalent column height of 1.5 cm (factor 0.33 for 4.5 cm and 0.5 for 3 cm). These measurements have already been corrected for the different distances to the focal plane of the instrument. The curve for low column height (1.5 cm) has a higher count rate up to a concentration of 200 ng/cm$^3$ than the other two curves. For these low concentrations, low column height data points suffer from a much higher systematic error than all other data points because much longer exposure times are needed to see the weak fluorescent signal. That means that a lot more stray-light counts occur as well, which leads to an overestimation of the count rate corresponding to this data point. It can also be seen that the 3.0 cm column height data differs from those of the other two in the regime above 400 ng/cm$^3$, which is probably a systematic error introduced by the focal distance correction. We conclude that the three area densities for the different column heights are equivalent to each other (after linear scaling). Figure 4 shows that the L.I.F.E. instrument measures area densities of pigments. Therefore, regardless of whether we measure a thin film or a column of a solution, the L.I.F.E. instrument is able to obtain comparable data.

Figure 5 shows the measured column density calibration curve derived from our data, which illustrates that the count rate scales linearly with a slope of 8.94 with respect to the column density. That means a count rate of 894 in a 1 s exposure equals an area density of 100 ng/cm$^2$. During the calibration, we reached a detection limit of 10 ng/cm$^2$ of phycoerythrin. For lower area densities, the stray light in the instrument is too strong to obtain meaningful data.

### *2.4. Mobility platform*

2.4.1. The Magma White rover. Magma White is an analog Mars rover developed as such by ABM Space Education. It has a 100 cm long, 90 cm wide, and 35 kg mobile platform made of plastic. It is capable of withstanding standard ambient temperatures in most of Earth's environments. The rover has six wheels with independent motors, non-steered, with six independent beams, secured with lightweight, temperature-resistant flexible bands. The deck

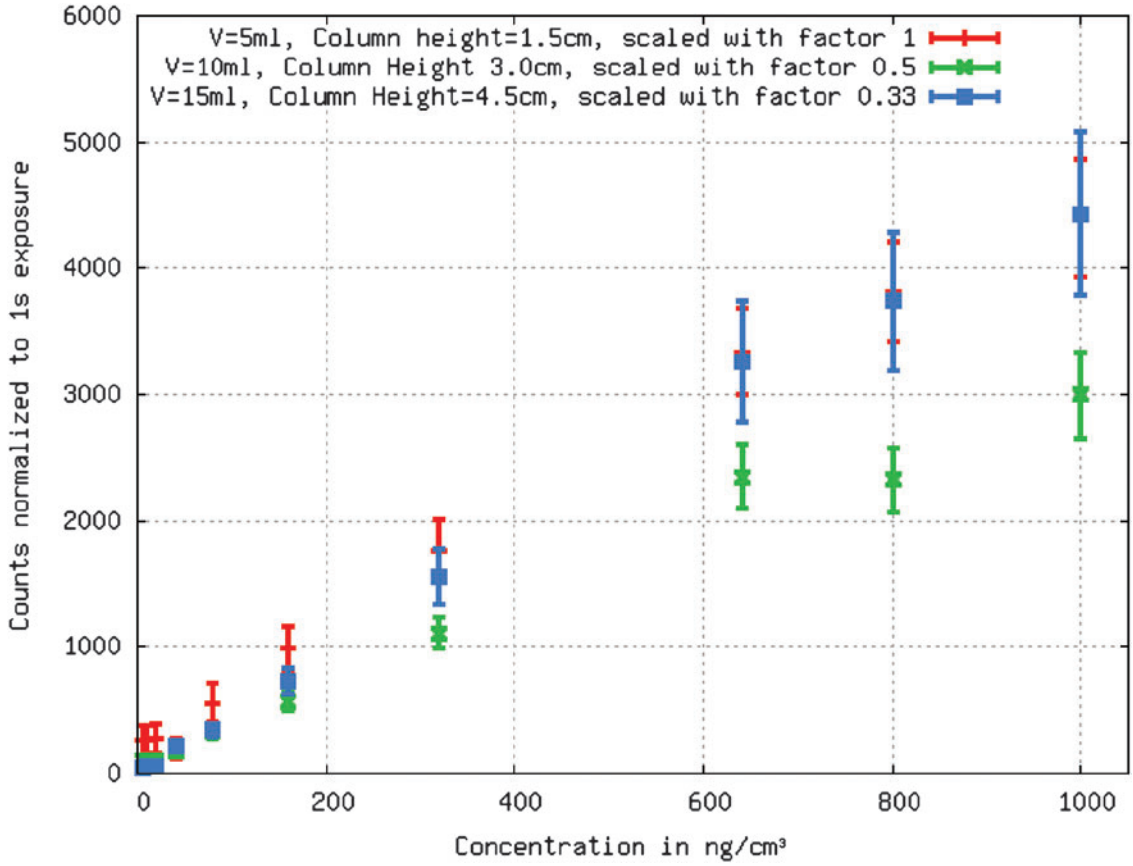


**FIG. 4.** Normalized count rates for the different column heights scaled to the equivalent column height of 1.5 cm (factor 0.33 for 4.5 cm and 0.5 for 3 cm). This figure shows that the count rate depends on the area density (column height × concentration) of the measured sample and not solely on the concentration. Color images available online at www.liebertonline.com/ast

allows installation of various accessories, including the main camera mast, main antenna mast, and the 3-stage robotic arm, all of which constitute the standard equipment. This equipment can be replaced by special payloads. The main computer system is located in the central trunk and is isolated from external conditions. Rover batteries allow operation for more than 6 h. Communication is accomplished over standard Internet protocols: Wi-Fi 5 GHz and 2.4 GHz frequency for diagnostics. Control software and interface are designed for Windows PC and Android smartphone. The range of rover operation depends on the type of antenna used. In Morocco, operation in a radius of up to 800 m from the antenna was successfully tested. The rover electronics are arranged in a modular fashion. This allows rapid reconfiguration of the platform for each expedition, payload, and experiment. The electronic modules are easily accessible and can be quickly replaced in case of potential failure or according to mission schedule requirement. In Morocco, some diagnostic and repair activities were successfully performed by OeWF personnel not familiar with the system, which were only tele-operated from the MSC. General functional blocks include power, computer, motor driver, communication, and camera. The voltage-generating module works in pulse mode to optimize power consumption. The onboard computer controls all execution and input modules. All other modules, such as camera or communication, can be replaced with analogous modules of different types (Wi-Fi, analog radio, BT, etc., and different types of cameras, sensors, etc.). The power and interface buses exhibit efficient throughput, which allows flexible adaptation to mission requirements. These useful characteristics result from experiences gained during the participation of the designers in the University Rover Challenge (Józefowicz and Meszyński, 2012) in the Utah deserts in the United States between 2009 and 2012. The hull is a structure that was derived from the adopted suspension model; it was designed by Wojciech Głażewski, who also designed two URC competition rovers from the Magma series. Design characteristics allow operation of the rover in rocky and sandy desert terrain in temperatures up to at least 40°C (tested) and on simulated regolith with slopes up to 40 degrees and rock fragments several centimeters in diameter. The rover can reach an average velocity of 5 km/h in easy desert terrain and has been previously tested on ice and snow surfaces. The purpose of this rover setup is to provide a platform to carry equipment and experiments developed for planetary exploration missions, such as arms, sampling tools, optical instruments, geophysical devices with antennas or electrodes, drills, scoops, penetrators, various cameras, as well as mechanical add-ons and alternative or auxiliary power sources. The flexible architecture, both of the structure and the electronics, allows connection and

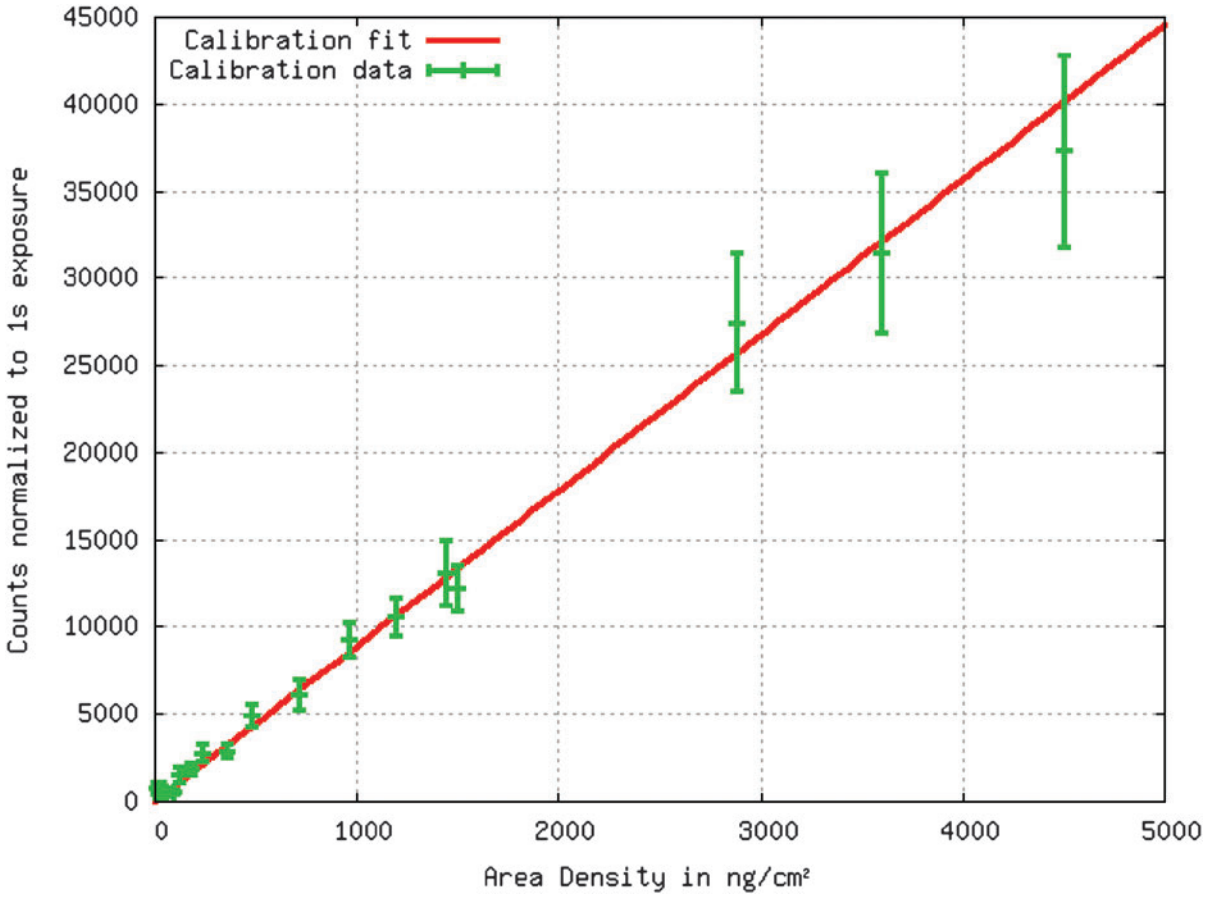


**FIG. 5.** Final calibration curve for phycoerythrin showing normalized counts over area density. Color images available online at www.liebertonline.com/ast

remote operation of multiple scientific devices up to 20 kg of total weight.

2.4.2. L.I.F.E. mounting platform. The L.I.F.E. instrument was installed in the front part of the rover (after removing the standard robotic arm, Fig. 6), on two servos that allow it to tilt from vertical position (-90 degrees in relation to the rover plane) to servo-off traveling position (+20 degrees in relation to the rover plane). This arrangement was chosen to allow a reasonably flexible approach to a target of interest. It does not allow movement to the sides, so the whole rover has to be turned. A control laptop connected directly to the rover's system was installed on the installation guides on the rover's deck.

## 3. Field Deployment and Preliminary Data

After deployment at the target site, the simulated rover operations were first performed from the Innsbruck MSC and the remaining sessions from Toruń through the MSC. All telemetry, video, and control data were available in all three locations. Two basic mission operation modes were employed: simulation (sim) by default including a 10 min time delay and non-sim. For non-sim activities, a natural signal, video, and command delay that was a result of the network and satellite band and link quality was present. In total, 11 runs of Magma White were performed, including 4 runs with L.I.F.E. as indicated in Table 1.

Sim mode indicates a full control over the instrument and the laser via the MSC, which was connected to the rover via satellite telemetry and telecommand. A mission was scored as a full success if three criteria were met: (a) the sample data acquisition went according to the predefined work flow, (b) data were obtained without touching the sample, and (c) a spectrum was acquired from the sample and received in the MSC via satellite link. Moderate success was defined as meeting two out of three of the criteria above. The primary objective was to tele-operate the Magma rover to a predefined target rock and take spectra with the L.I.F.E. instrument without human hands-on activity at the target site. In addition, 17 rock samples were acquired by the field crew, including in regions inaccessible for the robotic vehicle. The specimens were georeferenced and photodocumented at decreasing distances and increasing image resolution (scaled-observations work flow of Kereszturi, 2011). As an example, we present pilot measurements from a porous rock specimen collected on June 24, 2013, at 31°22.140N, 4°4.115W, about 1 km south of the Kess Kess Formation in an area devoid of fluvial structures (Fig. 7). The sample was then analyzed under laboratory conditions.

Figure 8 depicts the spectral response from the 405 and 532 nm laser illumination of the Sun-exposed side of a porous rock specimen measured with the L.I.F.E. instrument. The excitation time was 10 s at a distance of 16.5 cm for each laser. Figure 8A depicts the fluorescence spectrum of

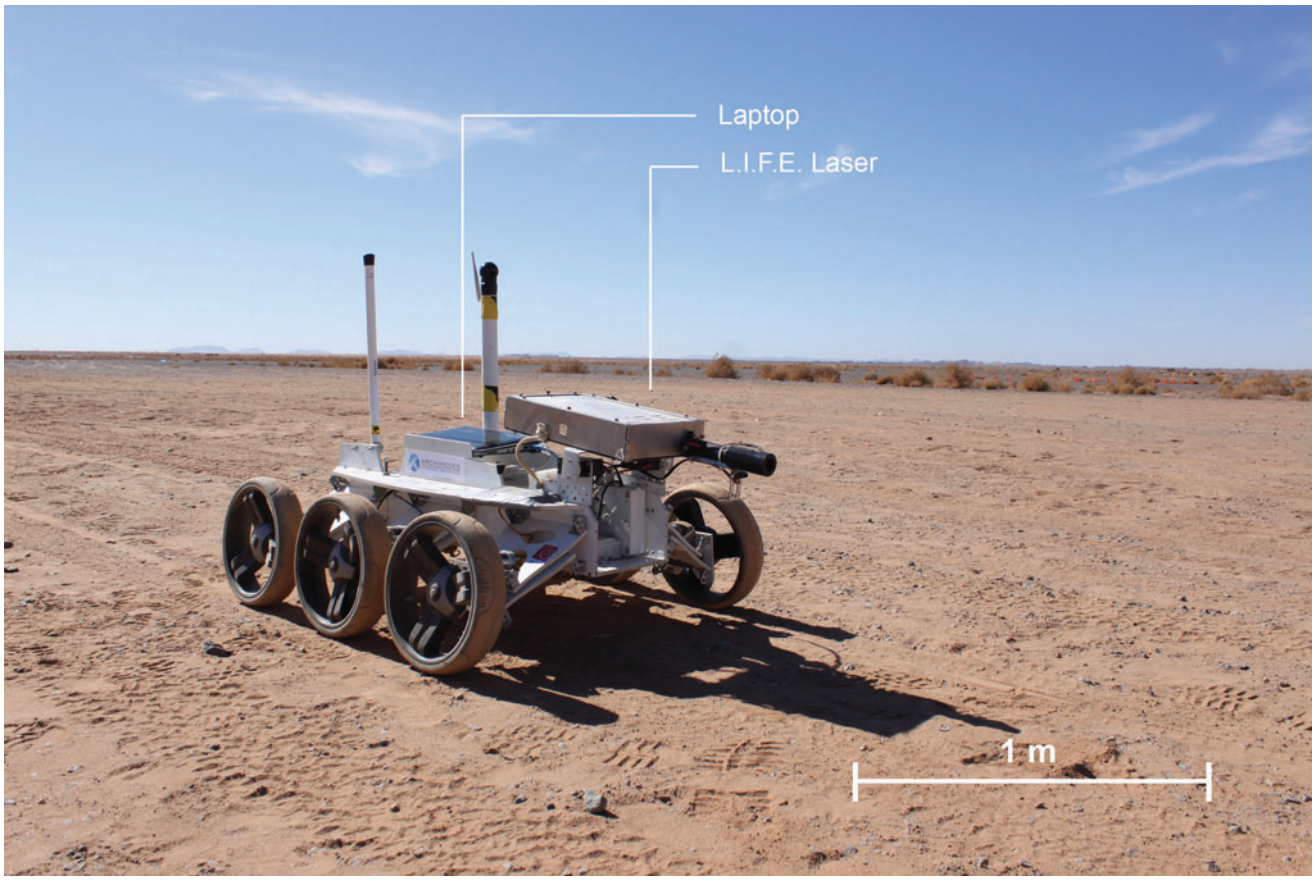


**FIG. 6.** The Magma Rover with the mounted L.I.F.E. instrument. Color images available online at www.liebertonline.com/ast

the rock after the 405 nm excitation. A broad fluorescence response can be seen. The central wavelength (CW) was determined by fitting a Gaussian line profile of 676.3 nm with a full width at half-maximum (FWHM) of 324 nm, which is in the right wavelength range for a detection of chlorophyll *a*. The very broad distribution can be explained by the low signal-to-noise ratio (S/N) of only 3. The low S/N is due to the fact that the interval between the sampling and laboratory analysis was 8 months, which led to a suspected deterioration of the chlorophyll. We infer that the maximum observed chlorophyll area density is 26.6 ng/cm$^2$.

The reduced chi-square of the fit was 0.9426. Figure 8B shows the response to the 532 nm excitation. Again, a broad fluorescence response can be seen. The CW has been determined to be 760.5 nm with a FWHM of 209.4 nm. This we consider to be too high for phycoerythrin, which would be expected to be closer to 600 nm. The S/N is around 18, and the reduced chi-square of the fit is 0.9843. This measurement is puzzling. It has the wrong wavelength signature for phycoerythrin, but it occurs at the same position as the chlorophyll detection. It could be a fluorescence of the stone itself.

Figure 9 depicts the spectral response of the shaded side of the same rock specimen. Again, the illumination time is 10 s. In Fig. 9A, after the 405 nm excitation, no fluorescence signal can be seen. We conclude that there is no chlorophyll on the shaded side of this rock. Figure 9B shows the response to the 532 nm excitation. Again, the peculiar fluorescence signal can be seen at a CW of 757.2 with a FWHM of 235.9 nm, of either mineral or organic origin.

We conclude that the Sun-exposed side shows a chlorophyll signal even after the stone was in storage for 8 months, while the shaded side shows no chlorophyll signal. We also measured a response following 532 nm excitation of either mineral or organic origin.

Table 1. L.I.F.E. Instrument Runs on the Magma White Rover during MARS2013

| *L.I.F.E. run ID* | *Magma run ID* | *Sim mode?* | *Terrain* | *Success level* | *Results/Notes* |
|---|---|---|---|---|---|
| A | 1 | No | Flat | Moderate | Basic telemetry and instrument status monitoring successful (power, position, context imagery); Sample approach algorithm requires additional development |
| B | 2 | No | Flat | Moderate | |
| C | 5 | Yes | Flat | Moderate | |
| D | Field lab | No | Flat | Success | Approach of rock successful, pointing mechanism demonstrated, data successfully transmitted. |


**FIG. 7.** Context overview of the sample collection site location 31°22.140N, 4°4.115W (Left). The sample (right image) is a porous rock collected and evaluated for fluorescence signatures on sunny and shady sides (see Fig. 8). In order to avoid confusion of a fluorescence signal from a mineralogical component, we compared the spectra obtained with the reference spectra of chlorophyll to exclude fluorescence from minerals. Color images available online at www.liebertonline.com/ast

## 4. Discussion

### 4.1. Field and tele-operational aspects

The terrain at the test site offered various inclinations and rock size-frequency distributions similar to the martian surface as encountered by the Mars Pathfinder rover and MOC boulder fields (Golombek *et al.,* 2003) and the Phoenix mission (Golombek *et al.,* 2008). For the purposes of the Magma White runs, it was locally categorized into ''easy'' (flat, hardened, and loose sand surface with fine gravels), ''moderate'' (loose sand and diversified gravel size, dry bushes present, periodical shallow stream beds, relatively poor Mars analogue), and ''hard'' (rocky hill slopes with inclination up to 50%, diversified rock sizes). Operations were performed during the day, with temperatures reaching +35°C. The rover was stored for the night in a nonheated tent, while the temperatures dropped to −4°C. Additional difficulties included the presence of fine dust and strong winds every 5–6 days. These led, for example, to the intrusion of dust particles into the laser system, which created image distortion. As a consequence, the field crew had to deploy an improvised dust-free area to open the sensitive instrument in the field, identify the particles, and remove them. Since the L.I.F.E. instrument was integrated with Magma White for the first time in the field, the team tele-operating the rover had to become familiar with the specificity of the instrument operation. First approaches to the samples were performed within the workshop tent. The team had to practice approaches and calibrate a mechanism for semiautonomous distance setting. This function, based on proximity sensor readings, made it possible to stop the tilting of the tip at an optimum distance from the sensed surface. Still, the surface itself—the rock—must be approached by the rover teleoperated by a human. For future work, an efficient, flexible, dedicated visual system for distance verification is a mandatory modification. Such a system was not available for the Morocco mission, which made the act of approaching a challenge.

### 4.2. Limitations of the method

The ultimate goal of this work was the deployment of the L.I.F.E. instrument in a wide area of habitats where logistical constraints have previously limited the collection of high-resolution data sets. These test runs with Magma White have provided significant observations that will guide the development of both the rover and the L.I.F.E. instrument. Constraints discerned with regard to the deployment of this spectrometer in a desert environment center on dust, temperature, mass, distance to target, and ambient light. Dust particles absorb and scatter both the laser beam and the target signal. But these small particles also readily enter the spectrometer itself. The repair performed by on-site investigators may not be an available option during use in certain sites of interest on Earth or on Mars. The pen laser beam focus was found to be susceptible to extreme temperature swings. As a result, diurnal temperature variations in the desert have to be taken into account. Total instrument mass reduction is essential for future implementations, since manipulating a solid one-piece instrument consumes much of the rover's power resources. A proper distance between the instrument tip and the probed surface is a critical measurement factor. Achieving this proper distance in a reliable way was the main challenge for the rover. Finally, ambient sunlight can swamp the laser signal and require a shading of the target or modifying the mission schedule to perform fluorescence experiments during evening and night cycles. Finally, to obtain the maximum flexibility during sample collection, several modifications are needed for the Magma White. In particular, the pointing mechanism for the rover instrument platform would benefit from more degrees of freedom and extended range of motion.

### 4.3. Potential of the method and outlook

As suggested by Davila and colleagues (2010), there are a variety of possibilities for deploying L.I.F.E. systems for noninvasive *in situ* exploration of remote extreme environments

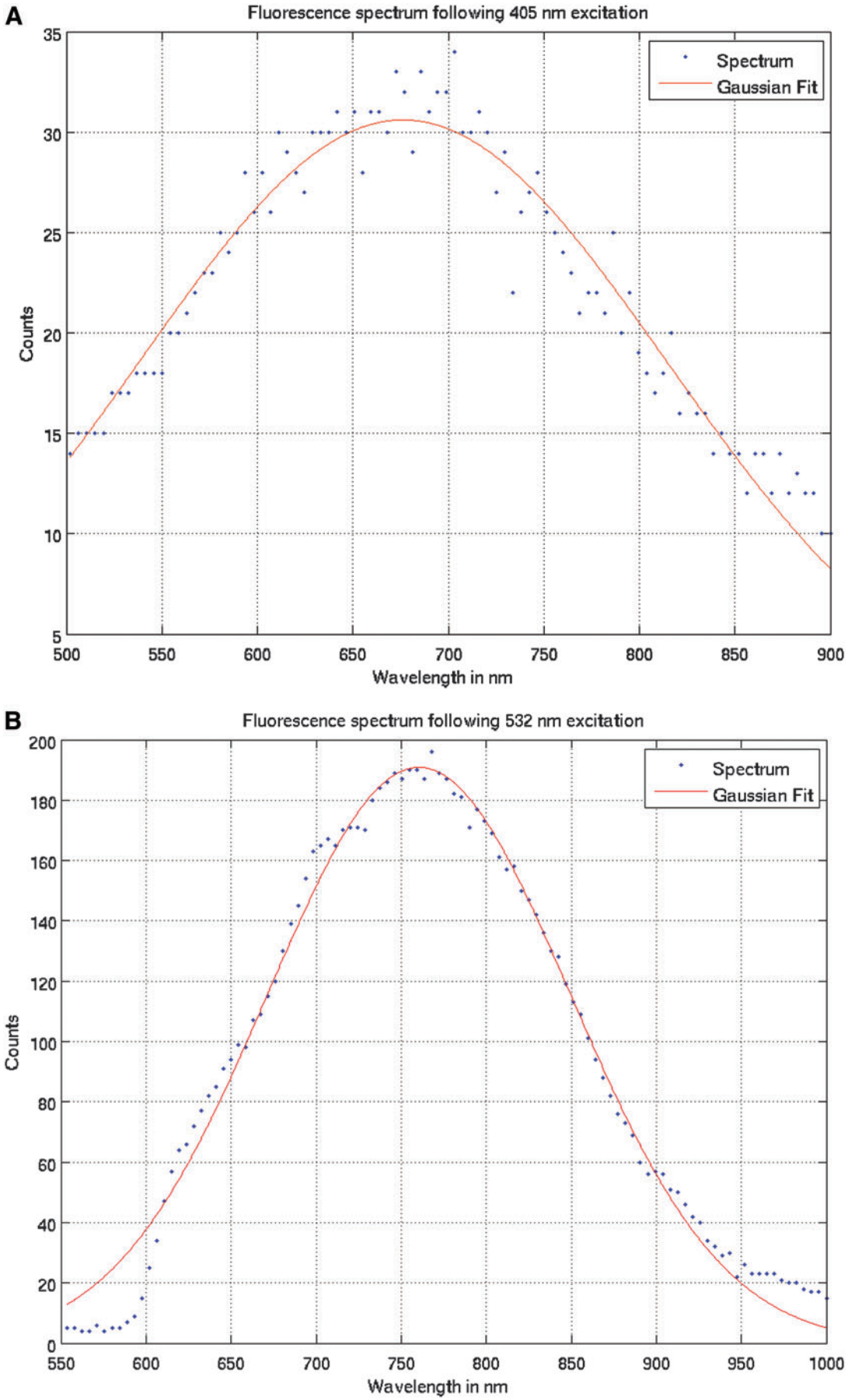


**FIG. 8.** (**A**) Fluorescence signal of the Sun-exposed side of the rock specimen after a 405 nm excitation. (**B**) Fluorescence signal after a 532 nm excitation. Color images available online at www.liebertonline.com/ast

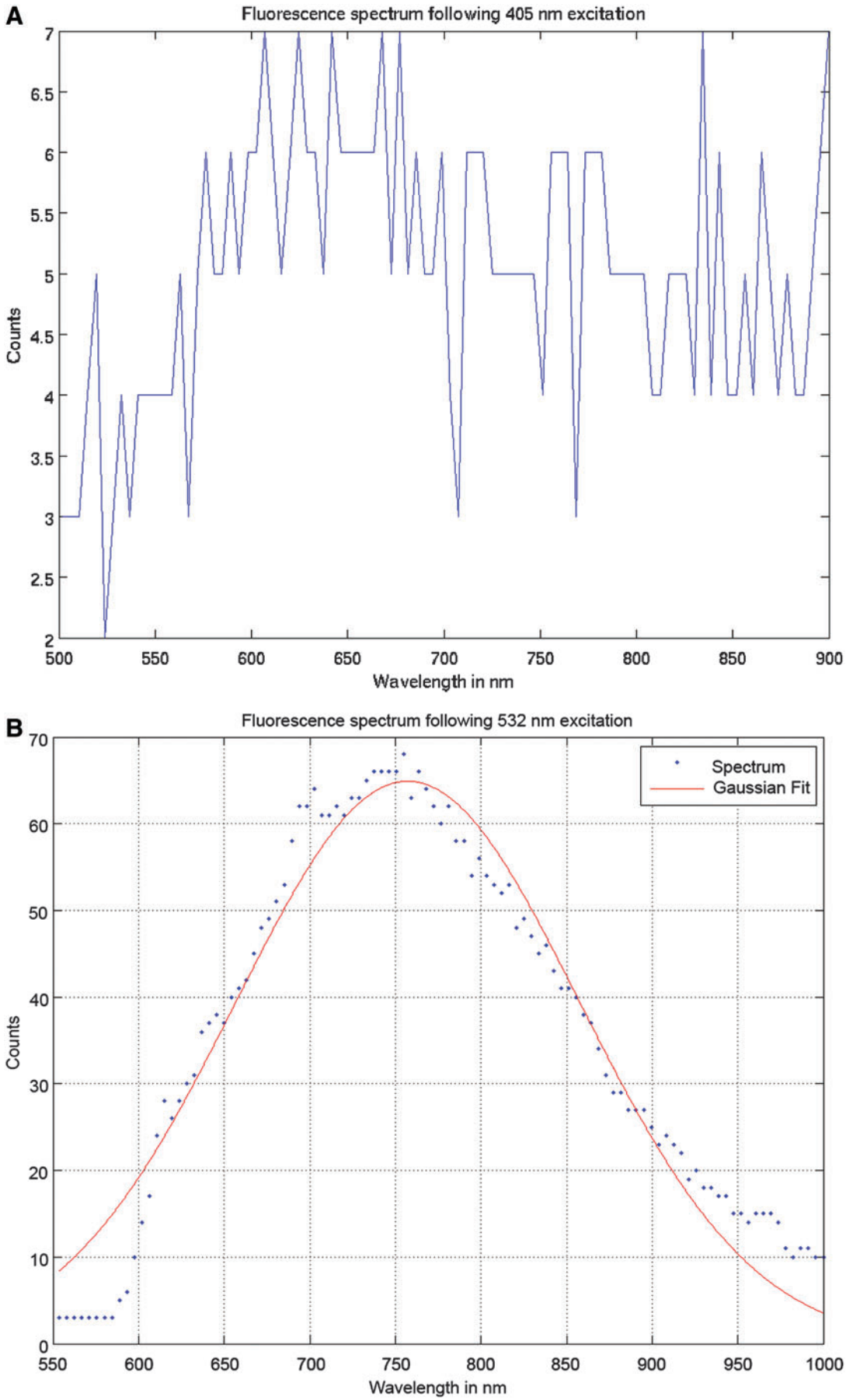


**FIG. 9.** (**A**) Fluorescence signal of the shaded side of the rock specimen after a 405 nm excitation. (**B**) Fluorescence signal of the shaded side after a 532 nm excitation. Color images available online at www.liebertonline.com/ast

on Earth and Mars. The L.I.F.E. instrument should be further tested on other Mars analog terrestrial environments such as the lava tubes in the Mojave Desert and the Arctic permafrost or glaciers.

While we expect the L.I.F.E. instrument will become an exceedingly useful new tool for the rapid nondestructive detection of photosynthetic pigments during extreme environment field work, proof of that must await the development of a substantial fluorescence database for mineral and organic targets for which both 405 and 532 nm probes are used. Although the data presented here on one target for demonstration purposes resembles the response we would expect from any of several species of carotenoids, biliproteins, or chlorophylls, the fluorescence could also have been generated by several different mineral species. For example, with 532 nm excitation, calcite can exhibit strong fluorescence between 600 and 620 nm attributed to the $Mn^{2+}$ activator (Gaft *et al.,* 2005). With 405 nm excitation, emerald can exhibit a broad fluorescence response centered between 720 and 730 nm attributed to the $Cr^{3+}$ activator (Barmarin, 2014). We consider construction of the data sets necessary for probabilistic classification of fluorescence activity in geobiological targets an effort of prime importance for implementation of L.I.F.E technology.

### Acknowledgments

The authors are thankful for support from the Austrian Federal Ministry for Science and Research, Sparkling Science Programme (SPA03-132 TriPolar, SPA04-147, CAVE.LIFE) to G.E.G. and B.S.; TAWANI Foundation, USA; Alpine Research Station Obergurgl (AFO-Grant to B.S.); and the Moroccan Ministry for Higher Education. This work has made use of the Austrian Space Forum Multi-Mission Data Archive (http://mission.oewf.org/archive). This work was supported by the Austrian Ministry of Science BMWF as part of the UniInfrastrukturprogramm of the Forschungsplattform Scientific Computing at Leopold-Franzens University Innsbruck, Austria. Support from the DK+ on computational interdisciplinary modeling is gratefully acknowledged.

### Author Disclosure Statement

The authors state no competing financial interest.

### Abbreviations

CW, central wavelength; FWHM, full width at half-maximum; L.I.F.E., laser-induced fluorescence emission; MSC, Mission Support Center; OeWF, Austrian Space Forum (Österreichisches Weltraum Forum); PAHs, polyaromatic hydrocarbons; S/N, signal-to-noise ratio; sim, simulation.

### References

Abedin, M.N., Bradley, A.T., Ismail, S., Sharma, S.K., and Sandford, S.P. (2013) Compact remote multisensing instrument for planetary surfaces and atmospheres characterization. *Appl Opt* 52:3116–3126.

Alimova, A., Katz, A., Savage, H.E., Shah, M., Minko, G., Will, D.V., Rosen, R.B., McCormick, S.A., and Alfano, R.R. (2003) Native fluorescence and excitation spectroscopic changes in *Bacillus subtilis* and *Staphylococcus aureus* bacteria subjected to conditions of starvation. *Appl Opt* 42:4080–4087.

Barmarin, G. (2014) *Online Database of Luminescent Minerals.* Available online at http://www.fluomin.org/uk/accueil.php.

Belka, Z. (1998) Early Devonian Kess-Kess carbonate mud mounds of the eastern Anti-Atlas (Morocco), and their relation to submarine hydrothermal venting. *Journal of Sedimentary Research* 68:368–377.

Bhatta, H., Goldys, E.M., and Learmonth, R. (2005) Rapid identification of microorganisms by intrinsic fluorescence. *Proc SPIE* 5699, doi:10.1117/12.588851.

Biemann, K., Oro, J., Toulmin, P., Orgel, L.E., Nier, A.O., Anderson, D.M., Simmonds, P.G., Flory, D., Diaz, A.V., Rushneck, D.R., and Biller, J.A. (1976) Search for organic and volatile inorganic compounds in two surface samples from the Chryse Planitia region of Mars. *Science* 194:72–76.

Bishop, J.L., Loizeau, D., Nancy, K., McKeown, N.K., Saper, L., Dyar, M.D., Des Marais, D.J., Parente, M., and Murchie, S.L. (2013) What the ancient phyllosilicates at Mawrth Vallis can tell us about possible habitability on early Mars. *Planet Space Sci* 86:130–149.

Bozlee, B.J., Misra, A.K., Sharma, S.K., and Ingram, M. (2005) Remote Raman and fluorescence studies of mineral samples. *Spectrochim Acta A Mol Biomol Spectrosc* 61:2342–2348.

Cavalazzi, B. (2006) Kess Kess carbonate mounds, Hamar Laghdad, Tafilalt, Anti-Atlas, SE Morocco—a field guide Morocco. UNESCO Field Action, 01–05 December 2006, UNESCO, Paris.

Cousins, C.R. and Crawford, I.A. (2011) Volcano-ice interaction as a microbial habitat on Earth and Mars. *Astrobiology* 11:695–710.

Dartnell, L.R., Desorgher, L., Ward, J.M., and Coates, A.J. (2007) Modelling the surface and subsurface martian radiation environment: implications for astrobiology. *Geophys Res Lett* 34:L02207.

Dartnell, L.R., Storrie-Lombardi, M.C., Mullineaux, C.W., Ruban, A.V., Wright, G., Griffiths, A.D., Muller, J.P., and Ward, J.M. (2011) Degradation of cyanobacterial biosignatures by ionizing radiation. *Astrobiology* 11:997–1016.

Dartnell, L.R., Patel, M.R., Storrie-Lombardi, M.C., Ward, J.M., and Muller, J.-P. (2012) Experimental determination of photostability and fluorescence-based detection of PAHs on the martian surface. *Meteorit Planet Sci* 47:806–819.

Davila, A.F., Skidmore, M., Fairén, A.G., Cockell, C., and Schulze-Makuch, D. (2010) New priorities in the robotic exploration of Mars: the case for *in situ* search for extant life. *Astrobiology* 10:1–6.

Farsund, O., Rustad, G., and Skogan, G. (2012) Standoff detection of biological agents using laser induced fluorescence—a comparison of 294 nm and 355 nm excitation wavelengths. *Biomed Opt Express* 3:2964–2975.

Fisher, T.M. and Schulze-Makuch, D. (2013) Nutrient and population dynamics in a subglacial reservoir: a simulation case study of the Blood Falls ecosystem with implications for astrobiology. *International Journal of Astrobiology* 12: 304–311.

Fisk, M.R., Storrie-Lombardi, M.C., Douglas, S., McDonald, G.D., and Popa, R. (2003) Evidence of biological activity in Hawaiian subsurface basalts. *Geochemistry, Geophysics, Geosystems* 4:1–24.

Gaft, M., Reisfeld, R., and Panczer, G. (2005) *Modern Luminescence Spectroscopy of Minerals and Materials,* Springer-Verlag, Berlin.

Gilichinsky, D., Rivkina, E., Shcherbakova, V., Laurinavchuis, K., and Tiedje, J. (2003) Supercooled water brines within permafrost—an unknown ecological niche for microorganisms: a model for astrobiology. *Astrobiology* 3:331–341.

Golombek, M.P., Haldemann, A.F.C., Forsberg, N.K., DiMaggio, E.N., Schroeder, R.D., Jakosky, B.M., Mellon, M.T., and Matijevic, J.R. (2003) Rock size-frequency distributions on Mars and implications for Mars Exploration Rover landing safety and operations. *J Geophys Res* 108, doi:10.1029/2002JE002035.

Golombek, M.P., Huertas, A., Marlow, J., McGrane, B., Klein, C., Martinez, M., Arvidson, R.E., Heet, T., Barry, L., Seelos, K., Adams, D., Li, W., Matijevic, J.R., Parker, T., Sizemoore, H.G., Mellon, M., McEwen, A.S., Tamppari, L.K., and Cheng, Y. (2008) Size-frequency distributions of rocks on the northern plains of Mars with special reference to Phoenix landing surfaces. *J Geophys Res Planets* 113, doi:10.1029/2007JE003065.

Groemer, G., Soucek, A., Frischauf, N., Stumptner, W., Ragonig, C., Sams, S., Bartenstein, T., Häuplik-Meusburger, S., Petrova, P., Evetts, S., and Sivenesan, C. (2014) The MARS2013 Mars analog mission. *Astrobiology* 14:360–376.

Hoge, F.E. and Swift, R.N. (1981) Airborne simultaneous spectroscopic detection of laser-induced water Raman backscatter and fluorescence from chlorophyll *a* and other naturally occurring pigments. *Appl Opt* 20:3197–3205.

Hoge, F.E., Wright, C.W., Kana, T.M., Swift, R.N., and Yungel, J.K. (1998) Spatial variability of oceanic phycoerythrin spectral types derived from airborne laser-induced fluorescence emissions. *Appl Opt* 37:4744–4749.

Jakosky, B.M. and Phillips, R.J. (2001) Mars' volatile and climate history. *Nature* 412:237–244.

Jepsen, S.M, Priscu, J.C., Grimm, R.E., and Bullock, M.A. (2007) The potential for lithoautotrophic life on Mars: application to shallow interfacial-water environments. *Astrobiology* 7:342–354.

Józefowicz, M. and Meszyński, S. (2010) Problematyka zawodów University Rover Challenge. Wybrane wytyczne dla robota operującego w warunkach pustynnych, PIAP.

Kereszturi, A. (2011) Geologic field work on Mars: distance and time issues during surface exploration. *Acta Astronaut* 68:1686–1701.

Leveille, R.J. and Datta, S. (2010) Lava tubes and basaltic caves as astrobiological targets on Earth and Mars: a review. *Planet Space Sci* 58:592–598.

McKay, C.P., Stoker, C.R., Glass, B.J., Davé, A.I., Davila, A.F., Heldmann, J.L., Marinova, M.M., Fairen, A.G., Quinn, R.C., Zacny, K.A., Paulsen, G., Smith, P.H., Parro, V., Andersen, D.T., Hecht, M.H., Lacelle, D., and Pollard, W.H. (2013) The Icebreaker Life mission to Mars: a search for biomolecular evidence for life. *Astrobiology* 13:334–353.

Mounji, D., Bourque, P.-A., and Savard, M.M. (1998) Hydrothermal origin of Devonian conical mounds (kess-kess) of Hamar Lakhdad Ridge, Antiatlas, Morocco. *Geology* 26:1123–1126.

Northup, D.E., Melim, L.A., Spilde, M.N., Hathaway, J.J.M., Garcia, M.G., Moya, M., Stone, F.D., Boston, P.J., Dapkevicius, M.L.N.E., and Riquelme, C. (2011) Lava cave microbial communities within mats and secondary mineral deposits: implications for life detection on other planets. *Astrobiology* 11:601–618.

Popa, R., Smith, A.R., Popa, R., Boone, J., and Fisk, M. (2012) Olivine-respiring bacteria isolated from the rock-ice interface in a lava tube cave—a Mars analog environment. *Astrobiology* 12:9–18.

Priscu, J.C. (2009) Life at the ends of the Earth. *Bioscience* 59:709–710.

Psenner, R. and Sattler, B. (1998) Life at the freezing point. *Science* 280:2073–2074.

Psenner, R., Wille, A., Priscu, J.C., Felip, M., Wagenbach, D., and Sattler, B. (2003) Low temperature environments and biodiversity. In ''Ice Ecosystems and Biodiversity.'' In *Knowledge for Sustainable Development (KSD): An Insight into the Encyclopaedia of Life Support Systems,* Vol. 3, UNESCO Publishing and Eolss Publishers, Oxford, UK, pp 573–598. Updated 2007.

Samsonoff, W.A. and MacColl, R. (2001) Biliproteins and phycobilisomes from cyanobacteria and red algae at the extremes of habitat. *Arch Microbiol* 176:400–405.

Sattler, B. and Storrie-Lombardi, M.C. (2009) L.I.F.E. in Antarctic lakes. In *Polar Microbiology: The Ecology, Biodiversity, and Bioremediation Potential of Microorganisms in Extremely Cold Environments*, edited by A.K. Bej, J. Aislabie, and R.M. Atlas, Taylor and Francis, London, pp 95–114.

Sattler, B., Puxbaum, H., and Psenner, R. (2001) Bacterial growth in supercooled cloud droplets. *Geophys Res Lett* 28:239–242.

Sattler, B., Storrie-Lombardi, M.C., Foreman, C.M., Tilg, M., and Psenner, R. (2010) Laser-induced fluorescence emission (LIFE) from Lake Fryxell (Antarctica) cryoconites. *Annals of Glaciology* 51:145–152.

Sharma, S.K., Misra, A.K., Lucey, P.G., and Lentz, R.C.F. (2009) A combined remote Raman and LIBS instrument for characterizing minerals with 532 nm laser excitation. *Spectrochim Acta A Mol Biomol Spectrosc* 73:468–476.

Skinner, J.A. and Mazzini, A. (2009) Martian mud volcanism: terrestrial analogs and implications for formational scenarios. *Marine and Petroleum Geology* 26:1866–1878.

Storrie-Lombardi, M.C. and Sattler, B. (2009a) Laser-induced fluorescence emission (L.I.F.E.): *in situ* nondestructive detection of microbial life in the ice covers of Antarctic lakes. *Astrobiology* 9:659–672.

Storrie-Lombardi, M.C. and Sattler, B. (2009b) Laser-induced fluorescence emission (L.I.F.E.): *in situ* and remote detection of life in Antarctic and Alaskan ice. *Proc SPIE* 7441, doi:10.1117/12.831288.

Storrie-Lombardi, M.C., Hug, W.F., McDonald, G.D., Tsapin, A.I., and Nealson, K.I. (2001) Hollow cathode ion laser for deep ultraviolet Raman spectroscopy and fluorescence imaging. *Rev Sci Instrum* 72:4452–4459.

Storrie-Lombardi, M.C., Muller, J.-P., Fisk, M.R., Griffiths, A.D., and Coates, A.J. (2008) Epifluorescence surveys of extreme environments using PanCam imaging systems: Antarctica and the Mars regolith. *Proc SPIE* 7097, doi:10.1117/12.800924.

Storrie-Lombardi, M.C., Muller, J.-P., Fisk, M.R., Cousins, C., Sattler, B., Griffiths, A.D., and Coates, A.J. (2009) Laser-induced fluorescence emission (L.I.F.E.): searching for Mars organics with a UV-enhanced PanCam. *Astrobiology* 9:953–964.

Storrie-Lombardi, M.C., Hall, A.P., Hang, S., Lyzenga, G.A., Clark, C.M., Sattler, B.I., Bej, A.K., and Hoover, R.B. (2011) Spectral profiling and imaging (SPI): extending L.I.F.E. technology for the Remote Exploration of Life in Ice Caves (R.E.L.I.C.) on Earth and Mars. *Proc SPIE* 8152, doi:10.1117/12.916987.

Stramski, D. and Kiefer, D.A. (1998) Can heterotrophic bacteria be important to marine light absorption? *J Plankton Res* 20:1489–1500.

Suo, Z., Avci, R., Schweitzer, M.H., and Deliorman, M. (2007) Porphyrin as an ideal biomarker in the search for extraterrestrial life. *Astrobiology* 7:605–615.

Tilg, M., Storrie-Lombardi, M., Kohstall, C., Trenkwalder, A., Psenner, R., and Sattler, B. (2011) L.I.F.E.: laser induced fluorescence emission, a non-invasive tool to detect photosynthetic pigments in glacial ecosystems. *Proc SPIE* 8152, doi:10.1117/12.893586.

Vítek, P., Edwards, H.G.M., Jehlicka, J., Ascaso, C., de los Ríos, A., Valea, S., Jorge-Villar, S.E., Davila, A.F., and Wierzchos, J. (2010) Microbial colonization of halite from the hyper-arid Atacama Desert studied by Raman spectroscopy. *Philos Trans A Math Phys Eng Sci* 368:3205–3221.

Warner, N.H. and Farmer, J.D. (2010) Subglacial hydrothermal alteration minerals in Jökulhlaup deposits of southern Iceland, with implications for detecting past or present habitable environments on Mars. *Astrobiology* 10:523–547.

Warren-Rhodes, K., Weinstein, S., Piatek, J.L., Dohm, J., Hock, A., Minkley, E., Pane, D., Ernst, L.A., Fisher, G., Emani, S., Waggoner, A.S., Cabrol, N.A., Wettergreen, D.S., Grin, E., Coppin, P., Diaz, C., Moersch, J., Ori, G.G., Smith, T., Stubbs, K., Thomas, G., Wagner, M., Wyatt, M., and Ng Boyle, L. (2007) Robotic ecological mapping: habitats and the search for life in the Atacama Desert. *J Geophys Res* 112, doi:10.1029/2006JG000301.

Wilhelm, R.C., Radtke, K.J., Mykytczuk, N.C.S., Greer, C.W., and Whyte, L.G. (2012) Life at the wedge: the activity and diversity of Arctic ice wedge microbial communities. *Astrobiology* 12:347–360.

Address correspondence to:
*Gernot Groemer*
*Austrian Space Forum*
*Sillufer 3a*
*6020 Innsbruck*
*Austria*

*E-mail:* gernot.groemer@oewf.org

Submitted 24 July 2013
Accepted 26 March 2014